CIDEP of 2-Chloroxanthone in 2-Propanol: Excitation Wavelength Dependence and Effect of Cross Relaxation

Yasutaka Kitahama,[†] Jung Sung Yang,[‡] and Noboru Hirota*,[†]

Department of Chemistry, Graduate School of Science, Kyoto University, Kyoto 606-8502, Japan, and Department of Chemistry, College of Natural Science, Kyungnam University, Masan 631-701, Korea

Received: January 27, 2000; In Final Form: March 30, 2000

The pattern of a chemically induced dynamic electron spin polarization (CIDEP) spectrum of 2-chloroxanthone (2-ClXn) in 2-propanol depends on the excitation wavelength. To clarify the cause of this intriguing phenomenon, we have investigated the details of the CIDEP and the transient visible absorption of 2-ClXn in 2-propanol produced by excitation at 355 or 308 nm. The CIDEP spectrum is strongly temperature dependent, which is mainly due to the temperature dependence of the net polarization. The net polarization consists of a fast rising emissive polarization and a slow rising absorptive polarization, both at 308 and 355 nm. However, the relative contributions of the two polarizations are different depending on the excitation wavelength, with more emissive polarization at 308 nm. From the analyses of the time profiles of the CIDEP signals and the results of quenching experiments with 2,6-di-*tert*-butylphenol, it is concluded that the emissive polarization arises from the triplet mechanism (TM) due to the reaction of highly excited 2-ClXn and the absorptive polarization arises from a slow reaction of the triplet molecules in thermal equilibrium. When excited at 355 nm the phase of the CIDEP spectrum of the 2-hydroxy-2-propyl radical due to the singlet−triplet mixing radical pair mechanism (ST_0M−RPM) is inverted at later times. It is shown by simulation that large inverted signals can be produced by the electron−nuclear cross relaxation mechanism under proper conditions.

Introduction

The time-resolved EPR technique has been applied to reveal photochemical reaction mechanisms through direct detection of transient paramagnetic species. The electron spin polarization of a transient species shows either an emission or an enhanced absorption of the microwave due to the transition between Zeeman split sublevels of a radical. This phenomenon is called chemically induced dynamic electron polarization (CIDEP). The CIDEP spectra have been usually accounted for in terms of a combination of two major mechanisms: the triplet mechanism (TM)[1,2] and the singlet−triplet ($S-T_0$) mixing radical pair mechanism (ST_0M−RPM),[3,4] established in 1970s. The TM yields spectra entirely in one phase, either absorption or emission, depending upon the manner of spin-selective intersystem crossing. The ST_0M−RPM has a characteristic that the low- and high-field halves of the spectra are in the opposite phase. However, it was recognized later that other mechanisms may play important roles in producing single-phase CIDEP signals such as TM. The suggested mechanisms include the $S-T_{\pm}$ mixing RPM,[5,6] the radical−triplet pair mechanism (RTPM),[7,8] the electron spin polarization transfer (ESPT),[9,10] and the spin−orbit coupling (SOC) induced polarization.[11,12] It has also been suggested that a reaction from a triplet state in thermal equilibrium produces a net absorptive polarization larger than that expected for a radical in thermal equilibrium.[13,14] Therefore, it is often not trivial to determine the exact CIDEP mechanism.

CIDEP spectra of carbonyl compounds have been investigated extensively, but there still remain some unsolved problems. For example, the question as to the mechanism to produce absorptive polarizations in some carbonyls, whether they are due to the TM or the reactions from triplet states in thermal equilibrium, has not been settled completely.[15,16] CIDEP of xanthone (Xn) gives an another example. It was recently found that the CIDEP spectra of Xn in alcohol solutions depend on the excitation wavelength. Excitation at 337 or 351 nm gives rise to CIDEP spectra of the Xn ketyl and alcohol radicals with E/A* (the low-field side is emissive and the high-field side is absorptive, where asterisk indicates the enhanced character) polarizations.[17,18] On the other hand, the spectra obtained by excitation at 308 nm are of the E*/A type.[19,20] Moreover, the spectra become completely absorptive on an addition of hydrochloric acid (HCl).[17,19] These observations suggest that different mechanisms to produce CIDEP are operative simultaneously in these systems, and the dominant mechanism varies depending on the experimental conditions such as the excitation wavelength, temperature, and delay time after laser excitation. However, the exact cause of the excitation wavelength dependence and the mechanism to produce the net absorptive polarization have not been made clear. It is noted that the excitation wavelength-dependent CIDEP has been observed before in the photolysis of [Ru(SnPh$_3$)(CH$_3$)(CO)$_2$(*N*,*N*′-diisopropyl-1,4-diazabutadiene)].[21] It was thought that this wavelength dependence was brought on by different routes of photodissociation of two distinct $\sigma\pi^*$ states.

Xanthone is a molecule of much spectroscopic and photochemical interest. Triplet xanthone (^{3}Xn) shows an unusual phenomenon of dual phosphorescence.[22,23] It is known that the $^3\pi\pi^*$ state is located close to the $^3n\pi^*$ state and the energy separation between them is sensitively affected by the environment.[23,24] Studies of photoexcited Xn have been performed with a variety of spectroscopic techniques such as transient absorption

* Corresponding author fax, +81-75-753-4000; e-mail, nhirota@ip.media.kyoto-u.ac.jp
† Kyoto University.
‡ Kyungnam University.

10.1021/jp0003205 CCC: $19.00
Published on Web 06/03/2000

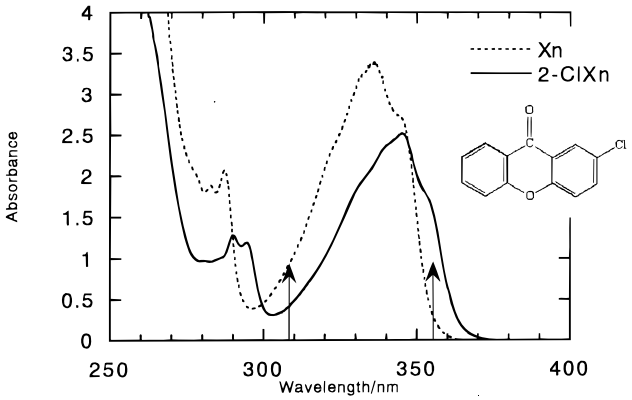

Figure 1. UV−visible absorption spectra of xanthone and 2-chloroxanthone in 2-propanol. The structural formula shows 2-chloroxanthone. Arrows indicate the wavelength of excitation.

spectroscopy in pico- and femtosecond time regions,[25] emission spectroscopy,[26] and magnetic resonance.[27,28] In view of the above-mentioned puzzling CIDEP behavior, it seems worthwhile to examine the CIDEP of xanthone further.

In this work, we have investigated CIDEP of 2-chloroxanthone (2-ClXn) in 2-propanol rather than xanthone itself, because 2-ClXn has a stronger absorption than xanthone at 355 nm (Figure 1). Its CIDEP spectrum shows excitation wavelength dependence similar to that found in Xn and yet shows a larger net absorptive polarization than Xn. Therefore, this system is better suited to study the net absorptive polarization in detail. To clarify the mechanisms to produce the CIDEP spectra, we have investigated the time profiles of the EPR signal intensities as well as those of transient absorption. We have attempted to simulate the time profiles of the EPR signals obtained by excitations both at 355 and 308 nm based on the model that the emissive polarization arises from the TM due to rapidly reacting triplet states, but the absorptive polarization originates from a slow reaction of triplet state molecules in thermal equilibrium. To support this model, we have also performed a quenching experiment with 2,6-di-*tert*-butylphenol. It is shown that the above two mechanisms are operative both at 355 and 308 nm, but the relative contributions of the two mechanisms are different at different excitation wavelengths.

In the course of this work, we also found that the E/A polarization pattern of the 2-hydroxy-2-propyl radical due to the ST_0M−RPM is inverted to the A/E pattern at later times. A similar phenomenon of polarization inversion was already observed in the case of *tert*-butyl radical formed by photolysis of di-*tert*-butyl ketone and 2-hydroxy-2-propyl radical formed by photolysis of acetone, and a mechanism involving the electron−nuclear cross relaxation was proposed to explain the phenomenon.[29] However, the relative intensities of the inverted signals observed in the present system are much stronger than those reported in the previous cases. Therefore, we have examined whether such a large polarization inversion can be explained in terms of the electron−nuclear cross relaxation.

Experimental Section

Continuous wave time-resolved EPR (TR-EPR) measurements were carried out with a modified X-band EPR spectrometer (JEOL FE−3X).[30] The CIDEP spectra were recorded with a boxcar integrator (PAR model 160 or Stanford Research System SR-250) whose gate width was 200 ns. A Nd:YAG laser (Quanta-Ray GCR-170, THG 355 nm, 10 Hz) or a XeCl excimer laser (Lambda Physik COMPex 102, 308 nm, 10 Hz) was used for photoexcitation. A digital oscilloscope (Tektronix TDS 520) was used for recording the time profiles of transient EPR signals. In recording the time profiles of transient EPR signals, measurements were made at resonance points, keeping the microwave power sufficiently low (0.1 mW) to avoid the effect of nutation. Transient absorption measurements were carried out with a lab-built spectrometer of conventional design using a Nd:YAG laser or a XeCl laser for photoexcitation.[31] UV−visible spectra were measured with a conventional spectrometer (Shimadzu UV-2500PC). 2-Chloroxanthone (2-ClXn) was purified by recrystallization from ethanol. 2-Propanol (2-PrOH), 2-propan(ol-*d*) ($(CH_3)_2CHOD$, 2-PrOD), and 2,6-di-*tert*-butylphenol (DTBP) were used as received (Nacalai Tesque, G.R. grade). The sample solution was deoxygenated by bubbling nitrogen gas during the experiments and flowed into a quartz flat cell (0.7 mL/minute). The concentration of 2-ClXn was 2×10^{-3} M (= mol dm^{-3}) in all experiments. The sample temperature was controlled with a cold nitrogen gas flow.

Results and Discussion

Overall Features of the CIDEP Spectra. The UV−visible spectrum of 2-ClXn in 2-PrOH is shown in Figure 1. The shape of the spectrum is very similar to that of Xn, but it is red-shifted by 10 nm from that of Xn. 355 nm is on the 0−0 band of the absorption spectrum, while 308 nm is on the short wavelength edge of the same absorption band. The TR-EPR spectra of radicals obtained at 1 μs after the laser excitation of 2-ClXn in 2-PrOH at 355 and 308 nm are given in Figure 2. The sharp and strong lines on the low- and high-field sides of the spectrum are due to the 2-hydroxy-2-propyl (HP) radical, and the multiline signal at the center of the spectrum is assigned to the 2-ClXn ketyl (2-ClXnH) radical. The protons at the 1, 3, 6, and 8 positions of the xanthone skeleton together with the OH proton produce the main hyperfine lines of the 2-ClXnH radical spectrum with an intensity ratio of approximately 1:5:10:10:5:1 at room temperature. The spectrum obtained by 355 nm excitation shows an E/A* polarization pattern that can be accounted for in terms of an E/A contribution generated by the ST_0M−RPM and a net absorptive component. When excited at 308 nm, the spectrum has a weaker absorptive component, making the spectrum pattern nearly E/A at room temperature. At −20 °C, the spectra show more stronger emissive components. The resolution of the hyperfine lines becomes poor, because the OH splitting no longer coincides with the other proton splittings at this temperature. The spectrum obtained by excitation at 308 nm becomes completely emissive at lower temperatures as shown in Figure 2d.

Figure 3 shows the spectra obtained at −50 °C with various delay times after the excitation by the Nd:YAG laser (355 nm). It is shown that the polarization pattern of the ketyl signal changes from E*/A at 0.5 μs after the laser pulse to nearly net absorption at later times. Therefore, it is considered that the emissive polarization shows a faster rise, but the absorptive polarization is produced more slowly. This suggests that two different CIDEP mechanisms are operative for net polarization, one giving a fast rising emissive polarization and the other giving a slowly developing absorptive polarization. The rise of the absorption cannot be due to the spin−lattice relaxation, because the rise rate becomes much faster than the spin−lattice relaxation rate at higher temperatures. The polarization of the HP radical on the low-field side changes from E to A at much later times. This phenomenon will be fully discussed in the final subsection.

Figure 4 shows the TR-EPR spectra of radicals generated by laser excitation of 2-ClXn in 2-PrOH in the presence of DTBP

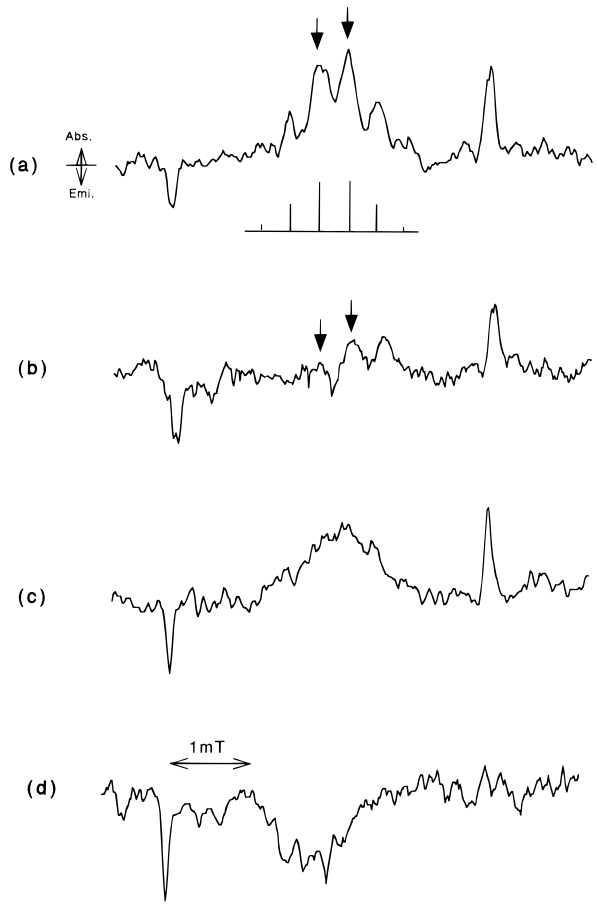

Figure 2. TR-EPR spectra observed in the photolysis of 2-ClXn in 2-propanol at 1 μs after excitation at (a) 355 nm and (b) 308 nm at room temperature. TR-EPR spectra at 1 μs after excitation at (c) 355 nm and (d) 308 nm at −20 °C. Arrows indicate peak positions of the of 2-ClXn ketyl radical signal where the time profiles shown in Figures 6 and 7 were taken. The stick diagram shows the main hyperfine structures of the 2-ClXn ketyl radical signal.

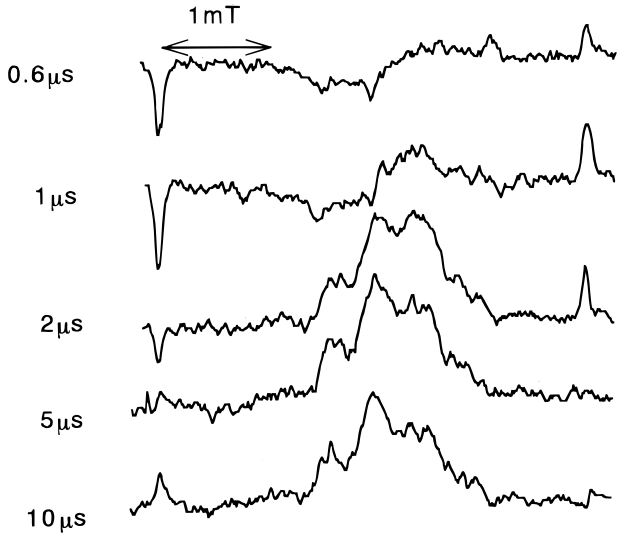

Figure 3. TR-EPR spectra observed in the photolysis of 2-ClXn in 2-propanol at various delay times after laser excitation at 355 nm at −50 °C.

(2×10^{-3} M and 2×10^{-2} M) at room temperature. Three sharp lines due to the phenoxyl radical produced from DTBP show an emissive polarization. At higher concentrations of DTBP the spectrum is dominated by the emissive signal of the phenoxyl radical (Figure 4c and d). The hydrogen abstraction

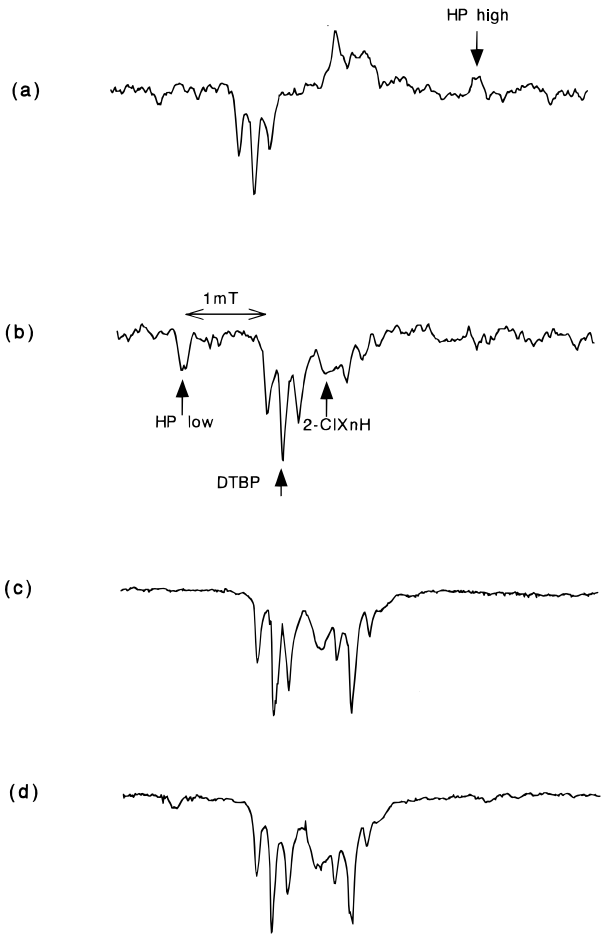

Figure 4. TR-EPR spectra observed in the photolysis of 2-ClXn in 2-propanol in the presence of 2×10^{-3} M of 2,6-di-*tert*-butylphenol at 1 μs after excitation at (a) 355 nm and (b) 308 nm. TR-EPR spectra observed in the photolysis of 2-ClXn in 2-propanol in the presence of 2×10^{-2} M of 2,6-di-*tert*-butylphenol at 1 μs after excitation at (c) 355 nm and (d) 308 nm. Arrows indicate the peaks at which the data given in Figure 8 were taken.

reaction giving the Xn ketyl radical and the phenoxyl radical is known to be very fast so that the polarization due to the TM is effective.[32] The observed spectra clearly show that the TM gives an emissive signal in this system. This is consistent with the prediction from the fact that the top sublevel is mostly populated in the intersystem crossing of an aromatic carbonyl.[27,28] Thus the emissive polarization observed at early times can be due to the TM, although the contribution from the RTPM cannot be excluded from the present experiments. On the other hand, the mechanism to produce the net absorptive polarization in this system cannot be due to the TM. The ESPT also cannot give an absorptive signal in this system, because the triplet state of 2-ClXn (^{3}2-ClXn) is emissive.[9,10] Neither the S−T-mixing RPM nor the RTPM produces an absorptive signal in this reaction from a triplet precursor and the negative sign of the exchange interaction, J.[5−8] Therefore, possible known mechanisms to produce the absorptive polarization are a reaction from triplet molecules in thermal equilibrium and the SOC-induced polarization.

Time Profiles of the EPR Lines of the 2-Chloroxanthone Ketyl Radical. Transient absorption experiments were carried out to determine the lifetime of ^{3}2-ClXn. Figure 5 shows the decay curves of the transient absorption at 600 nm following the photolysis of 2-ClXn in 2-PrOH at various temperatures by excitation at 308 nm. Similar decay curves were obtained by excitation at 355 nm. The decay curve consists of an initial fast

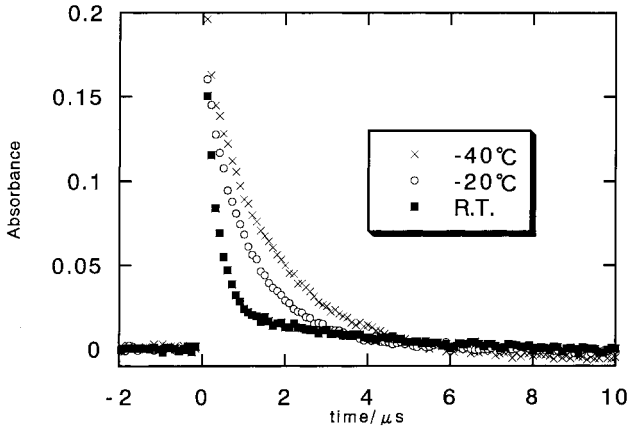

Figure 5. Decay curves of the transient absorption at 600 nm observed upon photoexcitation at 308 nm of 2-ClXn in 2-propanol at various temperatures.

exponential decay and a long-lived component. The long-lived component is attributed to the absorption by the 2-ClXnH radicals produced by hydrogen abstraction from solvent molecules. The fast component is assigned to the ^{3}2-ClXn decay. The obtained decay rate constants are 3.3×10^6 s^{-1}, 7.7×10^5 s^{-1}, and 5.6×10^5 s^{-1} at room temperature, -20 °C, and -40 °C, respectively. This decay component is considered to represent mainly the rate constant for the hydrogen abstraction reaction of ^{3}2-ClXn with 2-PrOH (k_{HA}). Since the quencher 2-PrOH is over excess in this system, it is reasonable to regard the hydrogen abstraction rate as the pseudo-first-order. The decay rate constant was found to be slightly dependent on the excitation wavelength. This difference, however, may be caused by the bimolecular quenching of triplet molecules, since the triplet concentrations are not identical in the experiments using different excitation wavelengths. It is important to note that the value of k_{HA} is on the order of 10^6 s^{-1} at room temperature, indicating that the hydrogen abstraction reaction is rather slow and the TM cannot be effective by this reaction. The value of k_{HA} is also temperature dependent and becomes much smaller at lower temperatures. At -40 °C, it is about 1/6 of the value at room temperature. The slow reaction rate is reasonable, because two electrons in the $^3\pi\pi^*$ state, the lowest excited ^{3}2-ClXn, are delocalized in the respective π and π^* molecular orbitals, and the direct hydrogen abstraction reaction by the carbonyl group is inefficient.

To obtain the information about the CIDEP mechanism, we consider the time profiles of the difference, $\Delta S(t)$, and the sum, $\Sigma S(t)$, of the EPR signal amplitudes of the $\pm M_I$ hyperfine lines. They give the time profiles of the ST_0M-RPM signal contribution and the net emissive or absorptive component, respectively. Here M_I is the nuclear spin magnetic quantum number. We discuss $\Delta S(t)$ and $\Sigma S(t)$ of the EPR signals of the 2-ClXnH radical in place of the HP radical, because the hyperfine lines of HP radical in the present experiments showed a large phase inversion at longer times, as shown in Figure 3. Measurements of $\Delta S(t)$ and $\Sigma S(t)$ were made at the peaks indicated by arrows shown in Figure 2. Since the g values of the present radicals are almost the same, g(HP radical) $= 2.0031$ and g(Xn ketyl radical) $= 2.003$, the Δg effect of the ST_0M-RPM can be safely neglected in the analysis.

The rise and decay of $\Delta S(t)$ are given by

$$\Delta S(t) = \frac{k_f P_{RPM}}{k_f - {}^R T_1^{-1}} \{\exp(-k_f t) - \exp(-t/{}^R T_1)\} \qquad (1)$$

Here P_{RPM} is the initial polarization (at $t = 0$) generated by geminate ST_0M-RPM. $^RT_1$ is the spin−lattice relaxation time of the 2-ClXnH radical, and k_f is the rate of the growth of the ST_0M-RPM signal. We ignore free-pair polarization created by radical termination reactions and assume $k_f > 1/{}^RT_1$.

We now consider mechanisms to give rise to a net emissive or absorptive signal which determines the time profile of $\Sigma S(t)$. We assume that the following three processes contribute to the signal. First, the hydrogen abstraction reaction indicated by the decay of the transient absorption represents the reaction of the triplet molecules in thermal equilibrium. This process gives an absorptive contribution. The signal is expected to rise with k_{HA} and decay with the spin−lattice relaxation rate of the radical, $1/{}^RT_1$. Second, radicals in thermal equilibrium give an absorptive signal. This signal is assumed to rise with $1/{}^RT_1$ and decay by the second-order recombination kinetics. Third, we assume that there is a fast reaction of ^{3}2-ClXn that gives rise to an emissive signal due to the TM. This reaction cannot be detected by our nanosecond transient absorption experiments. Since the response time of the spectrometer is much longer than the spin−lattice relaxation time of the triplet state, $^3T_1 = 6-25 \times 10^{-9}$ s,[33,34] the signal rises with k_{TM}, which is determined by the spectrometer response, and decays with $1/{}^RT_1$. The RTPM may make some contribution to the emissive polarization, but this contribution is not considered explicitly in the present analysis, because unknown parameters become too many by inclusion of this contribution. The time profile of $\Sigma S(t)$ is then given by the following equation:

$$\Sigma S(t) = \frac{k_{HA} P_{eq.T}}{k_{HA} - {}^R T_1^{-1}} \{\exp(-k_{HA} t) - \exp(-t/{}^R T_1)\} + P_{eq}[\{\exp(-t/{}^R T_1) - 1\}/(1 + n_0 k_d t)] + \frac{k_{TM} P_{TM}}{k_{TM} - {}^R T_1^{-1}} \{\exp(-k_{TM} t) - \exp(-t/{}^R T_1)\} \qquad (2)$$

Here k_d is the second-order reaction rate constant, and n_0 is the initial concentration of the radical. The conditions that $k_{HA} > 1/{}^RT_1$ and $k_{TM} > 1/{}^RT_1$ are assumed. We have simulated the time profiles using the values determined in the following way. The values of $^RT_1$ and k_{HA} were determined by the decays of $\Delta S(t)$ and the transient absorptions, respectively. We adjusted the value of $P_{eq.T}$ to be equal to $(4/3)P_{eq}$.[13,14] The simulation of $\Sigma S(t)$ was made by changing P_{TM}, P_{eq}, k_{TM}, and $n_0 k_d$. At room temperature, however, we used the ratios of P_{TM} to P_{eq}, which was estimated by the simulations at lower temperatures. Because k_{TM} estimated by the simulation at lower temperatures is much the same as k_{HA} at room temperature, it is impossible to analyze the time profiles at room temperature without fixing the values of P_{TM}/P_{eq}.

Figures 6 and 7 show $\Delta S(t)$ and $\Sigma S(t)$ obtained by excitations at 355 and 308 nm, respectively. $\Sigma S(t)$ strongly depends on the temperature. The simulated time profiles are shown as the lines in Figures 6 and 7. Though the signal-to-noise ratios of the observed time profiles are poor, we can reproduce the main qualitative features of $\Sigma S(t)$ at both 355 and 308 nm with reasonable values of parameters (Table 1) by a combination of the emission and the enhanced absorption whose rise becomes slower at lower temperatures as predicted by the temperature dependence of k_{HA}. At low temperatures, $\Sigma S(t)$ shows an emissive polarization in an early time region at 355 nm, but it becomes completely emissive in all the time region at 308 nm. Thus, the single phase polarizations of 2-ClXnH radical at both 355 and 308 nm are consistently explained by the same mechanism. It is concluded that the excitation wavelength

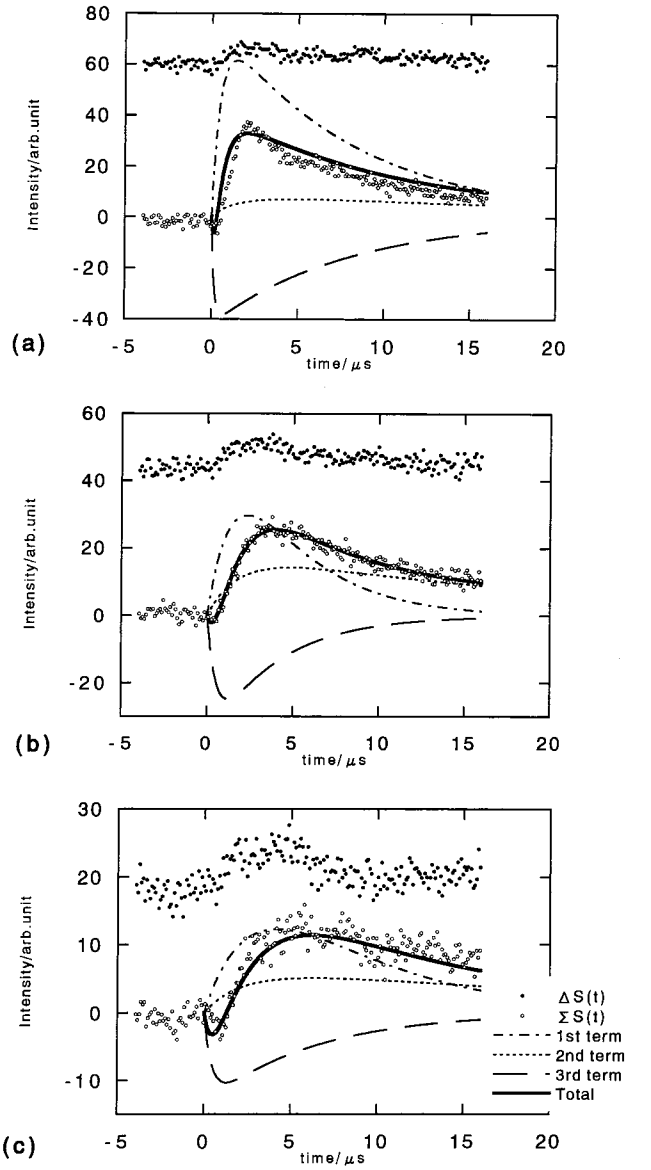

Figure 6. Time profiles of the difference, $\Delta S(t)$, and the sum, $\Sigma S(t)$, of the two peaks indicated by arrows in Figure 2 of the 2-ClXn ketyl radical signal obtained by excitation at 355 nm at (a) room temperature, (b) −20 °C, and (c) −40 °C. The closed and open circles indicate the observed $\Delta S(t)$ and $\Sigma S(t)$, respectively. The solid line represents the results of fitting to the data points of $\Sigma S(t)$ based on eq 2, which consist of the first term (− - −), the second term (- - - - - -), and the third term (− −). The initial values of $\Delta S(t)$ are displaced by (a) 60, (b) 40, and (c) 20, respectively.

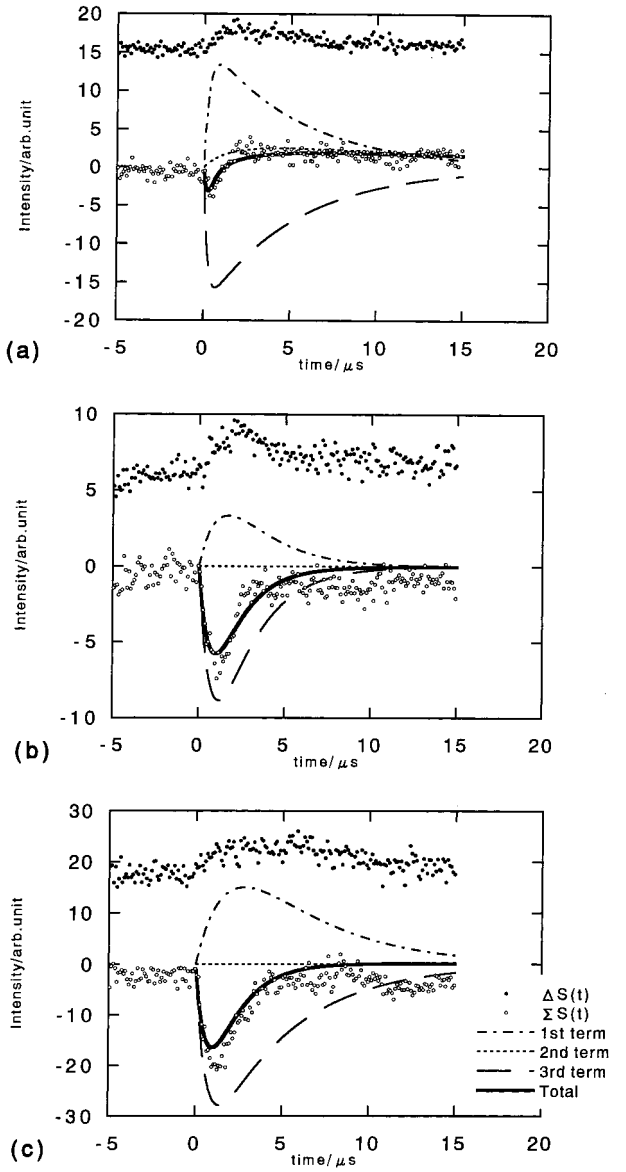

Figure 7. Time profiles of the difference, $\Delta S(t)$, and the sum, $\Sigma S(t)$, of the two peaks indicated by arrows in Figure 2 of the 2-ClXn ketyl radical signal obtained by excitation at 308 nm at (a) room temperature, (b) −20 °C, and (c) −40 °C. The meanings of the circles and lines are the same as given for Figure 6. The initial values of the $\Delta S(t)$ are displaced by (a) 15, (b) 5, and (c) 20, respectively.

dependence arises mainly from the difference in the relative intensities of the emissive polarization.

Quenching by 2,6-Di-*tert*-butylphenol. To gain further insight into the CIDEP mechanisms, we have studied the effect of quenching by DTBP in more detail. Figure 8 shows the changes of the polarizations and amplitudes of the radical signals produced by additions of DTBP. As the concentration of DTBP is increased, the emissive signal of the phenoxyl radical increases rapidly, accompanying the emissive polarization of the 2-ClXnH radical. This is clearly due to an increased contribution of the TM at higher concentrations of DTBP. The intensities of both high- and low-field peaks of the HP radical decrease rapidly on addition of small amounts of DTBP, but they approach constant values at high concentrations of DTBP. The trends of the intensity changes caused by the addition of DTBP are similar at both excitation wavelengths, but signals are always more emissive at 308 nm than at 355 nm. In Figure 8c, the net polarization of the HP radical (sum of the intensities of the low- and high-field peaks) measured at 1 μs after excitation at 355 and 308 nm are shown. At both excitation wavelengths, the net polarizations decrease by addition of 10^{-3} M of DTBP and reach constant values at higher concentrations of DTBP.

TABLE 1: Hydrogen Abstraction Rate Constant (k_{HA}), Spin−Lattice Relaxation Rate Constant of 2-Chloroxanthone Ketyl Radical ($^{R}T_1^{-1}$), and the Rise Constant of the Emission (k_{TM}) Used for Fitting to the Time Profiles of Transient Absorptions and TR-EPR Signals

	355 nm			308 nm		
	RT	−20 °C	−40 °C	RT	−20 °C	−40 °C
$k_{HA}/10^6\ s^{-1}$	2.0	0.67	0.33	3.3	0.77	0.56
$^{R}T_1^{-1}/10^6\ s^{-1}$	0.13	0.26	0.16	0.19	0.44	0.22
$k_{TM}/10^6\ s^{-1}$	6.6	1.9	2.2	3.9	1.5	1.7

The above observations are consistent with the polarization scheme deduced from the time profiles of the 2-ClXnH radicals.

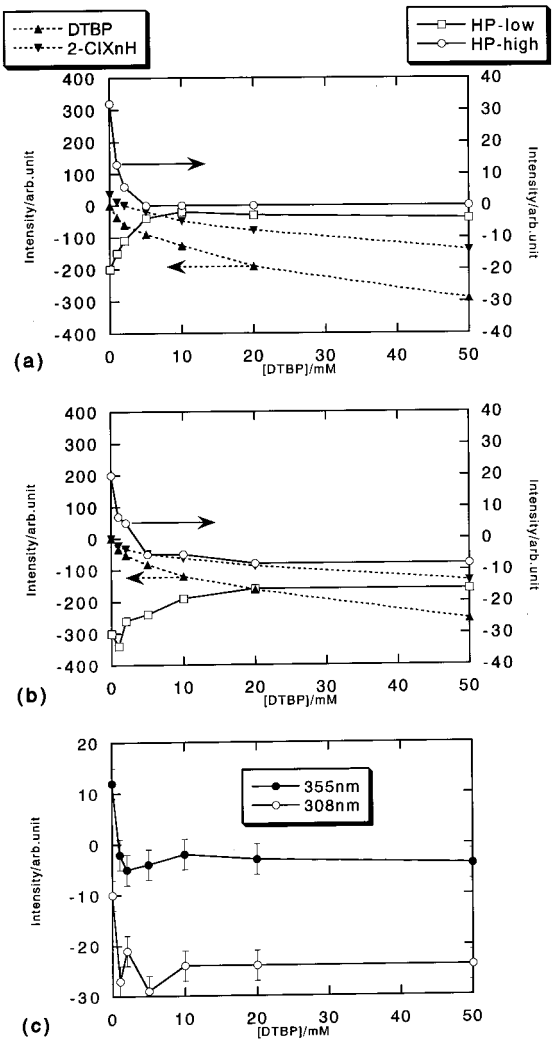

Figure 8. Dependence of the signal intensities of 2-ClXn ketyl radical, phenoxyl radical, and 2-hydroxy-2-propyl radical on the concentration of 2,6-di-*tert*-butylphenol. Data were taken at the peak positions shown in Figure 4 by excitation at (a) 355 nm and (b) 308 nm, and (c) gives the net polarization of 2-hydroxy-2-propyl radical.

The quenching of the triplet molecules is given by

$$\mathrm{d}[^3\text{2-ClXn}]/\mathrm{d}t = -k_Q[\text{DTBP}][^3\text{2-ClXn}] \qquad (3)$$

where k_Q is the quenching rate constant. Since the quenching reaction is considered to be diffusion controlled, k_Q is larger than 10^9 $M^{-1}s^{-1}$. Then ^{3}2-ClXn is quenched within 1 μs by an addition of 10^{-3} M of DTBP, inhibiting the slow reaction to produce the net absorptive polarization and leaving only the net emissive polarization due to the fast reaction. This explains the initial reduction of the intensities of the net polarization shown in Figure 8c. On the other hand, the net emissive polarization of the HP radical is not quenched by an addition of even 5×10^{-2} M of DTBP. This means that the emissive polarization is generated within 2×10^{-8} s, which is consistent with the TM. Thus, the results of the quenching experiments are consistent with the proposed CIDEP mechanism.

Reaction and CIDEP Mechanisms. The proposed CIDEP mechanisms are summarized in Figure 9a. It is considered that these mechanisms are common to excitations at both 355 and 308 nm, but the relative importance of the emissive polarization due to the TM is strongly enhanced at 308 nm. There are two remaining questions concerning these mechanisms. The first one

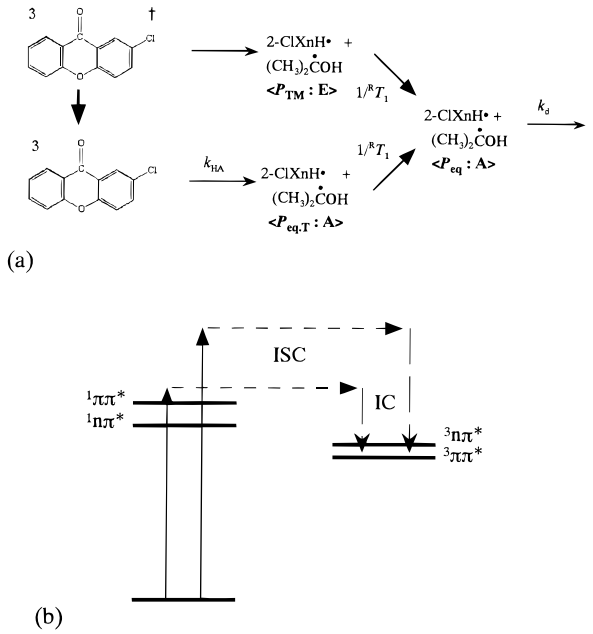

Figure 9. Schemes for (a) the generation of radicals by reactions and (b) the excitation. In (a), superscript dagger (†) indicates vibrationally highly excited ^{3}2-ClXn.

is why the emissive polarization is enhanced at 308 nm. The second one is about the reaction mechanism of the slow process.

We first discuss the question of the excitation wavelength dependence of the net emissive polarization. The experimental results given in the previous sections indicate that the excitation dependence is due to the difference in the efficiency of the TM produced by the fast reacting ^{3}2-ClXn. The 0−0 bands of $S_1(n\pi^*)$ and $S_2(\pi\pi^*)$ states of isolated 2-ClXn are located at 371.72 and 323.71 nm, respectively.[35] In 2-PrOH solution, however, the $S_2(\pi\pi^*)$ is red-shifted and 2-ClXn is excited to the $S_2(\pi\pi^*)$ state by the excitation both at 355 and 308 nm as seen from the absorption spectrum shown in Figure 1. The T_1 and T_2 states of 2-ClXn in 2-PrOH are $^3\pi\pi^*$ and $^3n\pi^*$ states, respectively. The intersystem crossing (ISC) in Xn is known to be very effective and this is also considered to be true in 2-ClXn. According to the usual El-Sayed's rule for the ISC, ^{3}2-ClXn-(T_1) is considered to be produced mainly by a combination of ISC and internal conversion (IC), $S_2(\pi\pi^*) \rightarrow$ (ISC) $T_2(n\pi^*) \rightarrow$ (IC) $T_1(\pi\pi^*)$ (Figure 9b). In the presence of high concentrations of DTBP shown in Figure 8, not only the net emissive but also the ST_0M-RPM polarizations of the HP radical (difference of the intensities of the low- and high-field peaks) obtained by excitation at 308 nm are larger than the one at 355 nm. Therefore, the difference in the TM activity appears to arise from the difference in the reactivities of the produced T_2 states: higher reactivities of the T_2 states with more vibrational energies. When the reaction rates of highly vibrationally excited T_2 states can compete with the vibrational relaxation rate, a larger TM polarization is observed. If the vibrational relaxation time is on the order of about 3×10^{-11} s, a reaction rate constant of the order of 10^{10} s^{-1} would be sufficient to produce such a polarization. When the second order hydrogen abstraction rate constant of highly vibrationally excited 2-ClXn is on the order of 10^9 $M^{-1}s^{-1}$, the pseudo-first-order rate constant k_{HA} becomes on the order of 10^{10} s^{-1}.

Next, we consider the mechanism of the slow reaction that gives rise to the absorptive polarization. Murai and Kuwata found that in the photolysis of Xn in ethanol by excitation at 351 nm the hydrogen atom in the hydroxy group is abstracted.[17]

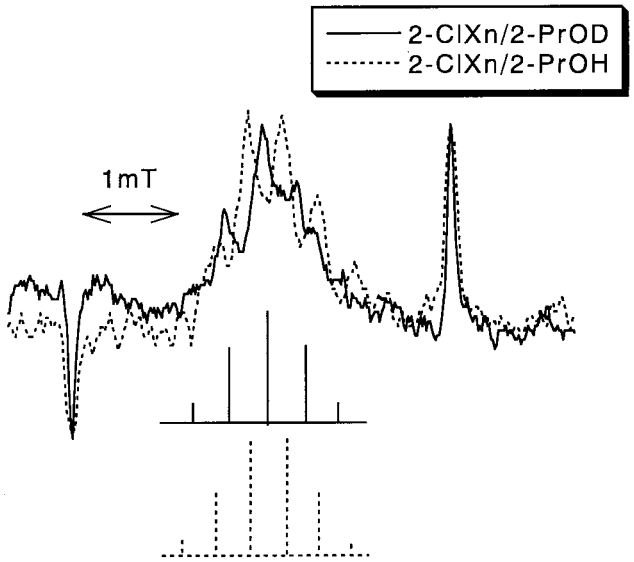

Figure 10. CIDEP spectra of 2-ClXn in 2-propan(ol-*d*) (solid line) and 2-propanol (broken line) at room temperature obtained by excitation at 355 nm. The stick diagram shows the main hyperfine structures of the 2-ClXnH and 2-ClXnD radical signal.

This is quite different from the usual hydrogen abstraction reaction of $^3n\pi^*$ carbonyls in which the CH hydrogen is abstracted. They proposed that an electron is initially transferred from ethanol to ^{3}Xn to form a transient charge-transferred complex, namely, a triplet contact radical pair, followed by an immediate transfer of a proton from the hydroxy group of the ethanol cation to the Xn anion.

We have examined whether this scheme is applicable to the present case. Figure 10 shows a comparison of the CIDEP spectrum of 2-ClXn in 2-PrOD obtained at 0.5 μs after laser excitation with that obtained in 2-PrOH. The hyperfine structures of the spectra did not change for 0.5−2.0 μs. The spectrum taken in 2-PrOD and that in 2-PrOH are definitely different, indicating that the proton in the hydroxy group in the ketyl radical is replaced by the deuteron in 2-PrOD at 355 nm. However, the alkoxy radical, $(CH_3)_2CHO\cdot$, was not found, because the alkoxy radical may react with the other 2-PrOH or 2-PrOD molecule very quickly and then change into an HP radical. The exchange of the hydrogen atom in the OH group of the 2-ClXnH radical with the deuterium of 2-PrOD is presumed to be much slower than 10^6 s^{-1}, because the spectra of the Xn ketyl radicals reported by Wilson[36] do not show any line-width effect expected for the rapid hydrogen exchange. Therefore, the mechanism involving a charge transferred intermediate state, namely, a triplet contact radical pair is also likely to be applicable to the slow reaction in the present system.

Then there is a possibility that the SOC-induced polarization proposed by Tero-Kubota's group is involved.[11,12] If back electron transfer from the upper spin sublevel of the triplet contact radical pair is faster than from the lower spin sublevels, due to the SOC interaction, this process may produce a radical with a larger absorptive polarization than $(4/3)P_{eq}$. The rise constant of the SOC-induced polarization will be equal to the generating rate constant of the triplet contact radical pair, namely, the quenching rate constant of ^{3}2-ClXn, k_{HA}, and will show the same temperature dependence. In simulating the time profiles of the 2-ClXnH radical signal, we assumed that $P_{eq.T}$ is equal to $(4/3)P_{eq}$. However, we can simulate the time profiles with $P_{eq.T}$ considerably larger than $(4/3)P_{eq}$. Since our signal-to-noise ratio is poor, it is not possible to quantitatively estimate the magnitudes of the absorptive polarization. Therefore, we cannot make a definite statement about the involvement of the SOC-induced polarization in the present system.

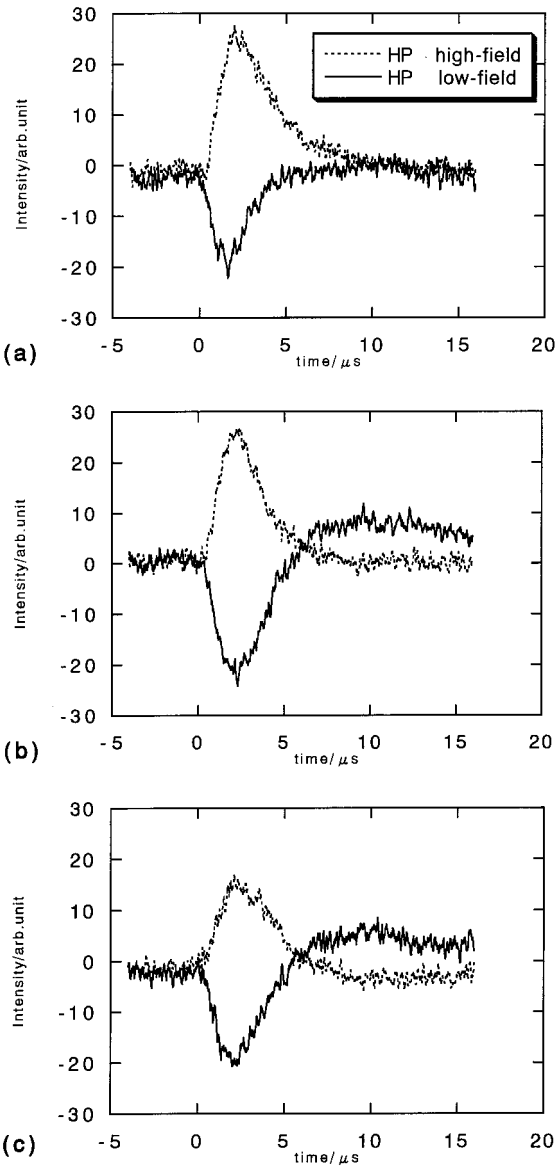

Figure 11. Time profiles of the $M_I = +1$ (low-field) and $M_I = -1$ (high field) peaks of the EPR signal of the HP radical obtained by excitation at 355 nm at (a) room temperature, (b) −20 °C, and (c) −40 °C.

Time Profiles of the EPR Lines of the 2-Hydroxy-2-propyl Radical. Figure 11 shows the time profiles of the $M_I = \pm 1$ hyperfine lines of the HP radical obtained by excitation at 355 nm. At lower temperatures, a remarkable phase inversion of the hyperfine lines from E/A to A/E was observed at longer times. In the case of excitation at 308 nm, it was difficult to detect the phase inversion because of a large emissive component.

Similar phenomena of phase inversion were already observed before.[37] Different sign of J in different radical pairs[38] and conversion of chemically induced dynamic nuclear polarization (CIDNP) into electron spin polarization via electron−nuclear cross relaxation[39] were proposed as the possible causes for the phase inversion. However, McLauchlan and Simpson claimed that only two cases, *tert*-butyl radical produced by photolysis of di-*tert*-butyl ketone and 2-hydroxy-2-propyl radical produced from acetone, showed genuine phase inversion.[40] Jent and Paul demonstrated that the phase inversion could be attributed to the

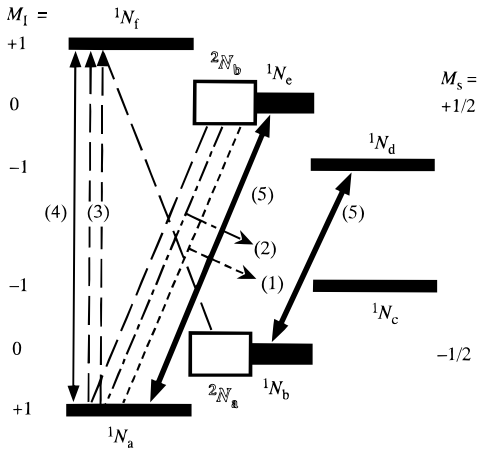

Figure 12. Schematic energy levels for a pair consisting of radical 1 carrying two equivalent protons with positive hyperfine interaction and radical 2 carrying no proton. Black and white boxes show the populations of radical 1 and 2, respectively. Arrows which are numbered show the reactions and transitions of the spin state a of radical 1 as explained in the text. Solid sloping arrows show the electron−nuclear cross relaxation ($\Delta M = 0$ transitions).

electron−nuclear cross relaxation and was not limited to the two ketone systems but could also occur for other radicals, when proper conditions were satisfied.[29] In this model, the nuclear spin polarization generated by CIDNP of the radical can be converted to the electron spin polarization via electron−nuclear cross relaxation.[29,39] This could generate an A/E polarization, if cross relaxation is dominated by $\Delta M = 0$ transitions ("flip-flop" processes) induced by modulation of the scalar hyperfine interaction. Transfer of magnetization from nuclei to an unpaired electron can be effective when nuclear magnetization is greatly amplified by CIDNP. Here we consider a radical carrying two equivalent protons with positive hyperfine interactions. When the populations of the radical whose $M_I = 0$ and $M_S = \pm 1/2$ (M_S is the electron spin magnetic quantum number) designated by $|0, +1/2\rangle$ and $|0, -1/2\rangle$ are larger than those of $|+1, -1/2\rangle$ and $|-1, +1/2\rangle$ states because of CIDNP, the $\Delta M = 0$ transitions (cross relaxation) mainly occur from $|0, +1/2\rangle$ and $|0, -1/2\rangle$ to $|+1, -1/2\rangle$ and $|-1, +1/2\rangle$, respectively. Populations of $|+1, -1/2\rangle$ and $|-1, +1/2\rangle$ become larger than those of $|+1, +1/2\rangle$ and $|-1, -1/2\rangle$, respectively. Then the A/E pattern polarization is produced (see black boxes in Figure 12).

In the present system, the relative intensities of the inverted signals with respect to the initial intensities are much stronger than previously observed. To see whether such large inverted signals can be produced by the cross relaxation mechanism, we have made a model calculation following the procedure by Jent and Paul.[29] We assume that our system can be represented by radical 1 ($\cdot RH_2$) carrying two equivalent protons with positive hyperfine interaction, corresponding to the HP radical, and radical 2 (R$\cdot$) carrying no proton, corresponding to the 2-ClXnH radical. Figure 12 shows the energy levels of the spin states for this pair. We assume the following processes. Reaction: (1) the singlet pair recombines with rate constant k, (2) the triplet pair reacts only to the extent that they experience $S-T_0$ mixing (rate constant kp_n). Generation of polarization: (3) the radical pairs which have different hyperfine energies are partially converted to other electron spin state due to the ST_0M-RPM (rate constant kp_e). Relaxations among the spin states of radicals are given by (4) electron spin−lattice relaxation (rate constant $1/T_1$) and (5) electron−nuclear cross relaxation (rate constant $1/T_x$). The populations of the six spin states, a−f, of radical 1 obey the following rate equations:

$$d^1N_a/dt = -k^1N_a{}^2N_b - kp_n{}^1N_a{}^2N_b - kp_e({}^1N_a{}^2N_b + {}^2N_a{}^1N_f) + \frac{{}^1N_f - \gamma^1N_a}{{}^1T_1(\gamma+1)} + \frac{{}^1N_e - 2\gamma^1N_a}{T_x(\gamma+1)} \quad (4)$$

$$d^1N_b/dt = -k^1N_b{}^2N_b + \frac{{}^1N_e - \gamma^1N_b}{{}^1T_1(\gamma+1)} + \frac{2^1N_d - \gamma^1N_b}{T_x(\gamma+1)} \quad (5)$$

$$d^1N_c/dt = -k^1N_c{}^2N_b - kp_n{}^1N_c{}^2N_b - kp_e(-{}^1N_c{}^2N_b - {}^2N_a{}^2N_d) + \frac{{}^1N_d - \gamma^1N_c}{{}^1T_1(\gamma+1)} \quad (6)$$

$$d^1N_d/dt = -k^2N_a{}^1N_d - kp_n{}^2N_a{}^1N_d - kp_e({}^2N_a{}^1N_d + {}^1N_c{}^2N_b) + \frac{\gamma^1N_c - {}^1N_d}{{}^1T_1(\gamma+1)} + \frac{\gamma^1N_b - 2^1N_d}{T_x(\gamma+1)} \quad (7)$$

$$d^1N_e/dt = -k^2N_a{}^1N_e + \frac{\gamma^1N_b - {}^1N_e}{{}^1T_1(\gamma+1)} + \frac{2\gamma^1N_a - {}^1N_e}{T_x(\gamma+1)} \quad (8)$$

$$d^1N_f/dt = -k^2N_a{}^1N_f - kp_n{}^2N_a{}^1N_f - kp_e(-{}^2N_a{}^1N_f - {}^1N_a{}^2N_b) + \frac{\gamma^1N_a - {}^1N_f}{{}^1T_1(\gamma+1)} \quad (9)$$

where γ is the EPR Bolzmann factor. Similar rate equations for a pair consisting of two $\cdot RH_2$ were already given by Jent and Paul.[29]

We have numerically integrated these equations to see if the observed phase inversion can be reproduced. We have first tried the calculation using $k = 3 \times 10^9$ $M^{-1}s^{-1}$; $p_n = 3 \times 10^{-2}$; $p_e = 3.5 \times 10^{-3}$, suggested by Jent and Paul,[29] and ${}^1T_1 = 2.7$ μs;[41] ${}^2T_1 = 7.0$ μs (estimated by the fitting as shown in Figures 6 and 7) with the initial condition ${}^1N_a = {}^1N_b/2 = {}^1N_c = {}^1N_d = {}^1N_c/2 = {}^1N_f$, ${}^2N_a = {}^2N_b$, and $\Sigma^1N_i = \Sigma^2N_i = 10^{-3}$ M. The calculation was made for ${}^1N_a(t) - {}^1N_f(t)$, low-field line, and ${}^1N_c(t) - {}^1N_d(t)$, high-field line by changing the value of T_x. The calculation could reproduce the inversion, but the relative intensities of the inverted signals were not so strong as observed. By decreasing the value of p_e to 1×10^{-3}, we could reproduce quite strong inverted signals as shown in Figure 13. The simulation shows that relatively large inverted signals are generated when the value of p_e/p_n is small, namely, the electron spin polarization due to the ST_0M-RPM is relatively small. A shorter T_x also produces larger inverted signals. The simulation on the pair consisting of two $\cdot RH_2$ indicated that the inverted signals are relatively weaker for this pair than for the pair consisting of $\cdot RH_2$ and R$\cdot$. However, the time profiles are also sensitive to the values of other parameters such as k and Σ^1N_i. Since there are so many parameters involved and our model is simple, the results of the simulation cannot be taken too seriously. Nevertheless, the simulation seems to indicates that large inverted signals can be obtained when proper conditions are met.

Conclusion

We conclude that the net polarizations of radicals generated by laser excitation of 2-ClXn in 2-PrOH are mainly due to three mechanisms as shown in Figure 9: (1) an enhanced absorption

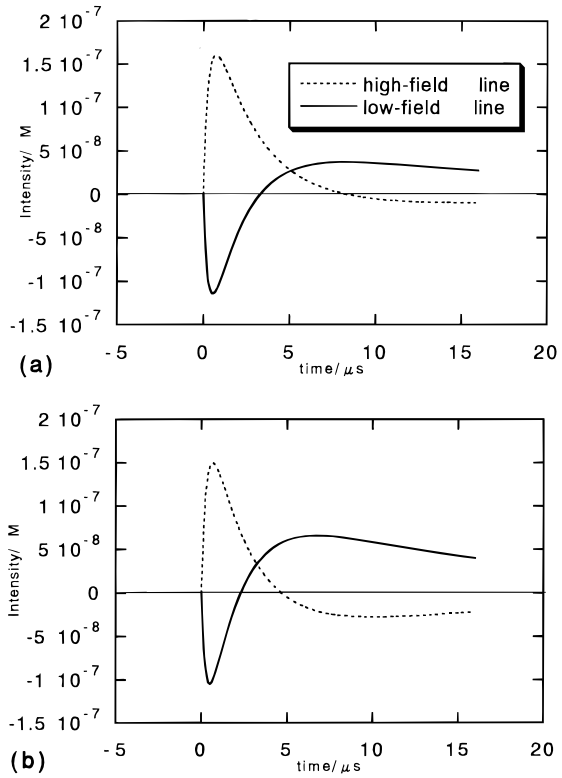

Figure 13. The calculated intensities of low- ($^1N_a - {}^1N_f$) and high-field line ($^1N_c - {}^1N_d$) of radical 1, corresponding to the HP radical, as a function of time for T_x = (a) 40 μs and (b) 20 μs.

due to the reaction from triplet state molecules in thermal equilibrium, (2) an absorptive polarization due to radicals in thermal equilibrium, and (3) an emissive TM polarization due to fast reaction of triplet molecules. The rise constant of the enhanced absorption is determined by the hydrogen abstraction reaction rate, k_{HA}, which is strongly temperature dependent. Therefore, the CIDEP spectrum is strongly affected by the temperature and the delay time after laser excitation. The contribution of the emissive TM polarization is larger by excitation at 308 nm than at 355 nm, probably because ^{3}2-ClXn can be excited to more reactive higher vibrationally excited states by excitation at 308 nm. On the other hand, the intensity of the enhanced absorption due to the reaction from thermally equilibrated triplet states is independent of the excitation wavelength. Therefore, the CIDEP pattern shows a striking excitation wavelength dependence. We believe that this conclusion is also applicable to the case of xanthone.

The signals of the HP radical are inverted from an E/A type to an A/E type at later times at low temperature. We have made a model calculation and showed that strong inverted signals can be produced by the electron−nuclear cross relaxation mechanism when proper conditions are met.

Acknowledgment. The authors are indebted to Professor S. Yamauchi of Tohoku University for his help in obtaining the TR-EPR spectra by excitation at 308 nm, and to Professor M. Baba for the data of the S_1 and S_2 states of 2-ClXn.

References and Notes

(1) Atkins, P. W.; Evans, G. T. *Mol. Phys.* **1974**, *27*, 1633.
(2) Pedersen, J. B.; Freed, J. H. *J. Chem. Phys.* **1975**, *62*, 1706.
(3) Adrian, F. J. *J. Chem. Phys.* **1971**, *54*, 3918.
(4) Pedersen, J. B.; Freed, J. H. *J. Chem. Phys.* **1973**, *58*, 2746.
(5) Trifunac, A. D.; Nelson, D. J.; Mottley, C. *J. Magn. Reson.* **1978**, *30*, 263.
(6) Adrian, F. J.; Monchick, L. *J. Chem. Phys.* **1979**, *71*, 2600.
(7) Blättler, C.; Jent, F.; Paul, H. *Chem. Phys. Lett.* **1990**, *166*, 375.
(8) Kawai, A.; Okutsu, T.; Obi, K. *J. Phys. Chem.* **1991**, *95*, 913.
(9) Imamura, T.; Onitsuka, O.; Obi, K. *J. Phys. Chem.* **1986**, *90*, 6241.
(10) Fujisawa, J.; Ishii, K.; Ohba, Y.; Iwaizumi, M.; Yamauchi, S. *J. Phys. Chem.* **1995**, *99*, 17082.
(11) Katsuki, A.; Akiyama, K.; Ikegami, Y.; Tero-Kubota, S. *J. Am. Chem. Soc.* **1994**, *116*, 12065.
(12) Katsuki, A.; Akiyama, K.; Tero-Kubota, S. *Bull. Chem. Soc. Jpn.* **1995**, *68*, 3383.
(13) Paul, H. *Chem. Phys.* **1979**, *40*, 265.
(14) Levstein, P. R.; van Willigen, H. *J. Chem. Phys.* **1991**, *95*, 900.
(15) Batchelor, S. N.; Kay, C. W. M.; McLauchlan, K. A.; Smith, P. D.; Yeung, M. T. *Mol. Phys.* **1994**, *82*, 325.
(16) Akiyama, K.; Sekiguchi, S.; Tero-Kubota, S. *J. Phys. Chem.* **1996**, *100*, 180.
(17) Murai, H.; Kuwata, K. *J. Phys. Chem.* **1991**, *95*, 6247.
(18) Koga, T.; Ohara, K.; Kuwata, K.; Murai, H. *J. Phys. Chem. A* **1997**, *101*, 8021.
(19) Sakaguchi, Y.; Hayashi, H.; Murai, H.; I'Haya, Y. J. *J. Am. Chem. Soc.* **1988**, *110*, 7479.
(20) Ohara, K.; Hirota, N.; Martino, D. M.; van Willigen, H. *J. Phys. Chem. A* **1998**, *102*, 5433.
(21) Kleverlaan, C. J.; Martino, D. M.; van Slageren, J.; van Willigen, H.; Stufkens, D. J.; Oskam, A. *Appl. Magn. Reson.* **1998**, *15*, 203.
(22) Yang, N. C.; Murov, S. L. *J. Chem. Phys.* **1966**, *45*, 4358.
(23) (a) Connors, R. E.; Christian, W. R. *J. Phys. Chem.* **1982**, *86*, 1524. (b) Long, M. E.; Lim, E. C. *Chem. Phys. Lett.* **1973**, *20*, 413. (c) Pownall, H. J.; Huber, J. R. *J. Am. Chem. Soc.* **1971**, *93*, 6429. (d) Connors, R. E.; Walsh, P. S. *Chem. Phys. Lett.* **1977**, *52*, 436.
(24) Scaiano, J. C. *J. Am. Chem. Soc.* **1982**, *102*, 7747.
(25) Cavaleri, J. J.; Prater, K.; Bowman, R. M. *Chem. Phys. Lett.* **1996**, *259*, 495.
(26) (a) Vala, M.; Hurst, J.; Trabjerg, I. *Mol. Phys.* **1976**, *31*, 1393. (b) Baba, M.; Kamei, T.; Kiritani, M.; Yamauchi, S.; Hirota, N. *Chem. Phys. Lett.* **1991**, *185*, 354. (c) Koyanagi, M.; Terada, T.; Nakashima, N. *J. Chem. Phys.* **1988**, *89*, 7349.
(27) Murai, H.; Minami, M.; I'Haya, Y. J. *J. Phys. Chem.* **1988**, *92*, 2120.
(28) Chakrabarti, A.; Hirota, N. *J. Phys. Chem.* **1976**, *80*, 2966.
(29) Jent, F.; Paul, H. *Chem. Phys. Lett.* **1989**, *160*, 632.
(30) Yamauchi, S.; Hirota, N. *J. Phys. Chem.* **1984**, *88*, 4631.
(31) Ohara, K.; Hirota, N. *Bull. Chem. Soc. Jpn.* **1996**, *69*, 1517.
(32) Ishiwata, N.; Murai, H.; Kuwata, K. *Res. Chem. Intermed.* **1993**, *19*, 59.
(33) Hore, P. J.; Joslin, C. G.; McLauchlan, K. A. *Chem. Soc. Rev.* **1979**, *8*, 29.
(34) Ohara, K.; Murai, H.; Kuwata, K. *Bull. Chem. Soc. Jpn.* **1992**, *65*, 1672.
(35) Ohshima, Y.; Fujii, T.; Baba, M., private communication.
(36) Wilson, R. *J. Chem. Soc. B* **1968**, 1581.
(37) (a) Basu, S.; Grant, A. I.; McLauchlan, K. A. *Chem. Phys. Lett.* **1983**, *67*, 517. (b) McLauchlan, K. A.; Stevens, D. G. *J. Magn. Reson.* **1985**, *63*, 473. (c) McLauchlan, K. A.; Stevens, D. G. *J. Chem. Soc., Faraday Trans. 1* **1987**, *83*, 29.
(38) Carmichael, I.; Paul, H. *Chem. Phys. Lett.* **1979**, *67*, 519.
(39) Valyaev, V. I.; Molin, Yu. N.; Sagdeev, R. Z.; Hore, P. J.; McLauchlan, K. A.; Simpson, N. J. K. *Mol. Phys.* **1988**, *63*, 891.
(40) McLauchlan, K. A.; Simpson, N. J. K. *Chem. Phys. Lett.* **1989**, *154*, 550.
(41) Tominaga, K.; Yamauchi, S.; Hirota, N. *J. Chem. Phys.* **1990**, *92*, 5175.